Indian Journal of Engineering & Materials Sciences
Vol. 25, April 2018, pp. 163-168

Analysis of formability and twist angle in AA5052 alloy by single point incremental forming process

V Mugendiran[a]* & A Gnanavelbabu[b]

[a]Department of Production Technology, MIT Campus, Anna University, Chennai 600 044, India
[b]Department of Industrial Engineering, CEG Campus, Anna University, Chennai 600 025, India

Received 15 February 2016; accepted 16 June 2017

The incremental forming process is highly characterized by its degree of flexibility and mainly suggested for rapid prototyping. Formability of the sheet metal mainly depends on the properties of the metal sheet, forming process and forming conditions. This paper focuses on the development of FLD for AA5052 alloy at room temperature. In this study a truncated square pyramid is formed by single point incremental process. The formed part was analyzed for its formability and thickness distribution along with the twist induced during incremental forming process. To evaluate the system accuracy a numerical model of a truncated square pyramid is developed by means of FE simulation code Abaqus and validated experimentally. The assessment of finite element simulation with experimental work shows a good agreement between the computed and measured values. The angle of twist is less at lower and more at higher forming heights.

Keywords: Incremental forming, Forming limit diagram, Numerical analysis, Twist angle

Incremental forming is a new technique that is feasible to control the formability of sheet metals. Single point incremental forming process is mainly applied in forming complex external shapes and profiles over metal sheets using a hemispherical round tool. Powel and Andrew[1] introduced incremental forming process first. It is very appropriate and economical for rapid prototyping in contrast to the conventional forming process[2,3]. The tool moves in the pre-determined paths and deforms the sheet metal locally into desired shapes. In SPIF, the local deformation imposed by the tool on the work-piece is limited to the forming zone alone and is the combination of stretching and shearing[4,5]. Few salient features of this forming process are easy adaptability, reduced tooling cost and easily programmed. The process has applied in automotive applications and biomedical sectors[6]. For waste sheet metal recycling this process can be adopted. Various authors have analyzed the formability in incremental sheet forming. For various strain conditions, Filice *et al.*[7] have predicted the forming limit diagram. Park and Kim[5] and Fratini *et al.*[6,7] compared the formability diagram of SPIF with conventional one. The results show that the forming limit diagram obtained by SPIF than forming limit diagram by hemispherical dome test. Due to the local deformation mechanism, sheet metal thinning occurs during SPIF. The obtained wall thickness after forming becomes less than that of the initial blank sheet. Further the sheet fracture occurs somewhere in between 0° and 90°. Iseki *et al.*[8] studied the effect of tool path, increment per revolution of tool, and material properties on the forming limit. It is obivious from his contribution that the forming limit is enhanced with a decreasing vertical displacement increment of the tool or tool step; that the principal strain path is almost linear; that the ratio of strains is roughly equal to the number of paths; and that the forming limit line is expressed by e_1+e_2=fracture strain due to incremental forming in plane-strain. In incremental forming, compressive strain is repeatedly applied so void growth and coalescence are suppressed and localization of strain is prevented. Many researchers have reported the forming parameters like spindle speed, tool feed and step depth, surface quality[9,10], geometric accuracy[11], forming forces[9,12,13] and thinning[14]. In this present study, AA 5052 aluminium alloy sheet was studied since it was widely used in aeronautics and automotive industries. The material properties, formability, thickness distribution and the twist angle developed through single point incremental forming process were analyzed. Since incremental forming, characterized by localized strains and displacements, an explicit approach solution has been adopted for numerical analysis[15]. The finite element model has

been created using Abaqus/Explicit to analyze and compare the experimental work carried out.

Materials and Methodology

Material and mechanical properties

In the present study, AA5052 aluminium alloy was selected in the form of sheet, which was obtained by rolling process[16,17]. The experiments were carried out on a sheet metal of thickness 1 mm whose chemical composition is given in Table 1.

According to ASTM E8/E8 M-09 standard tensile test specimens were prepared in the rolling direction (0°), diagonal direction (45° to rolling direction) and transverse-in-plane direction (90° to rolling direction) and tests were conducted to determine the mechanical properties[18,19]. The strain hardening exponent (n) and the plastic strain ratio (r) are the factors that determines the formability sheet metals. The specimen was fractured under displacement control at a constant strain rate of 0.1 mm/min. Typical mechanical properties of AA5052 alloy obtained from uniaxial tension tests are given in Table 2.

The true stress-strain curves describing the working hardening behaviour for each orientation are shown in Fig. 1. It is evident from the Fig.1 to use an isotropic yield model than the anisotropic model. Therefore an elasto-plastic model with an isotropic yield criterion, a non-linear kinematic hardening model and associated flow rule was considered[20]. The flow hardening law was given by

$$\sigma = K\varepsilon^{n} \quad \text{... (1)}$$

where σ represents the applied stress, K strength coefficient, n the work hardening exponent and ε are the accumulated plastic strain

Table 1 — Chemical composition of Al 5052 alloy both nominal and actual (weight %)[10]

Composition	Mg	Cr	Si	Fe	Cu	Mn	Zn	Al
Nominal	2.23	0.18	0.14	0.31	0.01	0.05	0.001	Rem
Actual	2.2-2.8	0.15-0.35	0.25 Max	0.40 Max	0.10 Max	0.10 Max	0.10 Max	

Table 2 — Derived mechanical properties of AA5052 alloy

Direction	YS (MPa)	UTS (MPa)	Elongation (%)	'n'	'K'	'r'
0°	236.0	267.4	13.2	0.1575	417.04	1.0310
45°	246.8	273.7	13.2	0.1414	405.12	1.9357
90°	243.9	275.3	12.4	0.1589	431.87	0.8410
Average	243.38	272.53	13.0	0.1498	414.79	1.4358

Experimental set-up

The experiments were performed using a computer controlled 3-axis milling machine. The experimental set-up including a clamping plate along with backing plate with a square hole of sized 115 mm × 115 mm was used as shown in Fig. 2[21]. The initial blank square sheet of 150 mm × 150 mm with a working area of 110 mm × 110 mm was used. The sheet was laser etched with a series of circular grids of 5 mm diameter on one side to allow the deformation strains to be measured after forming. A simple tool made of high speed steel with

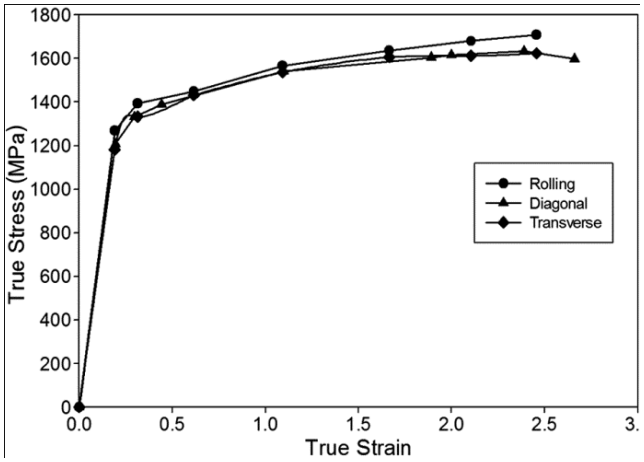

Fig. 1 — True stress-true strain curve for different orientation

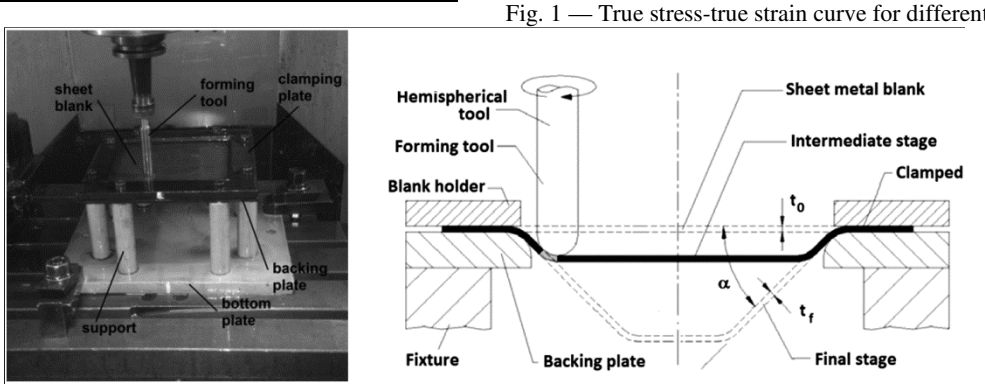

Fig. 2 — Experimental setup and crossectional view

hemispherical end of 12 mm diameter was used to form the parts. The feed rate was set at 240 mm/min with a vertical step depth of 0.5 mm. The spindle speed was chosen as 1930 rpm[10]. The geometry used in this study was a truncated square pyramid (Fig. 3a). The desired tool path was chosen carefully such that it does not leave any marks over the sheet metal surface (Fig. 3b). The wall angle for formation was taken as 70°. Engine oil was used as lubricant between the tool and the work-piece.

Formability was measured by the deformed major and minor axis of the ellipses obtained from the etched circles over the sheet metal. During forming the circle grids get deformed. The deveiation of the deformed circle from the original values are measured and the principal strains resulting from the major and minor directions are calculated. The values of strain were computed from

$$\varepsilon_1 = In\left(\frac{a}{d}\right) and \varepsilon_2 = In\left(\frac{b}{d}\right) \quad \ldots (2)$$

where '*d*' denotes the original diameter of the circle grid and '*a*' and '*b*' denote the major and minor axis of the ellipse. The resulting forming limit curve was plotted by taking the principal strains ($\varepsilon_1 and \varepsilon_2$) at failure from grid elements adjacent to the crack formed area[22].

Explicit method is suitable for numerical analyzes of simple geometries. A three dimensional elastic-plastic finite element model was established for an incremental forming process using Abaqus/Explicit[23]. The hardening behavior was described by Swift's law as $\sigma = \varepsilon k^n$.The material assigned with isotropic property and was meshed with four noded doubly curved shell elements and a 3D 4 noded rigid elements (R3D4) for tooling; with six Gaussian integration points through the thickness were used[15]. These elements are well suited for the study of thickness variations through the deformation process. To reduce the element size, an adaptive approach of mesh refinement has been adopted when the distortion level reaches a maximum value[23]. The element sizes are selected in a manner that satisfies convergences, computational cost and accurate results. The friction coefficient for the lubricated condition is assigned as 0.16 between contact surfaces. Corresponding boundary conditions were defined to make the tool to move in the desired path. Penalty approach was applied and master-slave kinematic contact interaction properties was being adopted.

Results and Discussion

The component was formed until crack on the surface of the specimen occurred. A total height of 67 mm was obtained before the crack occurred. The formed component has been shown in Fig. 4. Figure 5

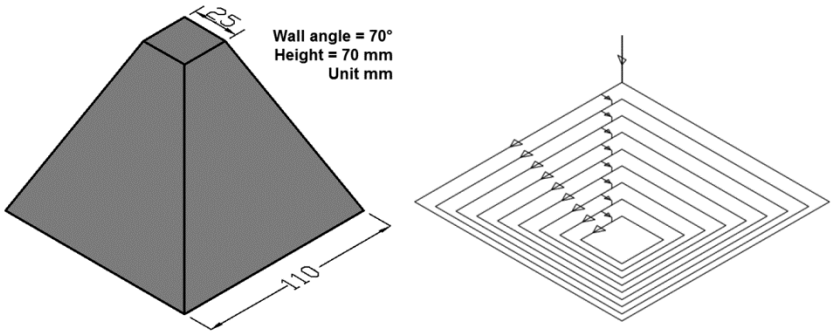

Fig. 3 — (a) Targeted component and (b) tool path used

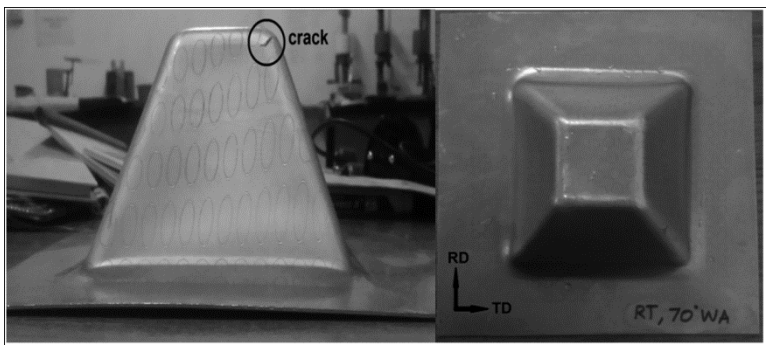

Fig. 4 — Formed component (a) front view and (b) top view

shows the detailed view of designed and formed component. It can be noticed that there was a deviation of the formed part at the corner and centre portion from the originally designed part and also the centre portion of the formed part due to the spring back effect developed during the metal forming processes. Due to the residual stresses developed during the forming process, a compressive stress was developed which makes the sheet metal drawn towards the centre, creating a curved spring back effect. The comparison between the targeted and formed shape is shown in Fig. 5a. The plotted forming limit diagram was shown in Fig. 5b for component formed using single point incremental forming process.

Incremental forming process was fully characterized by local deformation happening between the work-piece and the rotating tool. The process area was mainly subjected to stretching and shear deformation. As a result, mathematically the ultimate sheet thickness can be obtained by using the sine law.

$$t = t_0 \sin\alpha \quad \ldots (3)$$

where t_0 is the initial sheet thickness, t is the ultimate sheet thickness and α is the wall angle[23]. According to the equation, the major parameter affecting the wall thinning is wall angle. Variation in thickness was measured along the line over the formed surface as shown in Fig. 6.

Numerical simulations are shown in Fig. 7. The outputs indicate that the sheet metal undergoes plane deformation, compressing in the normal direction and stretching in the radial direction nearer the edges and biaxial stretching on the surfaces of the formed slant

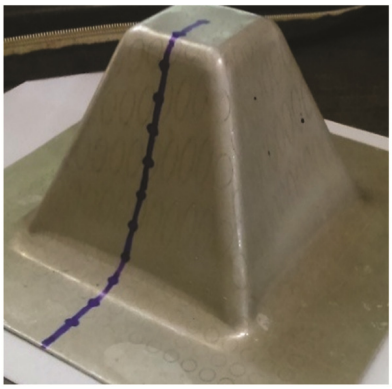

Fig. 6 — Thickness measured at various points on formed surface

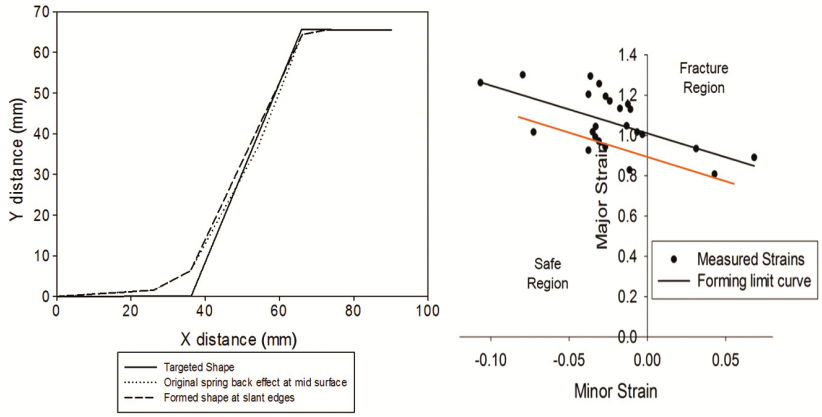

Fig. 5 — (a) Detailed view of designed and formed shapes and (b) the obtained FLD

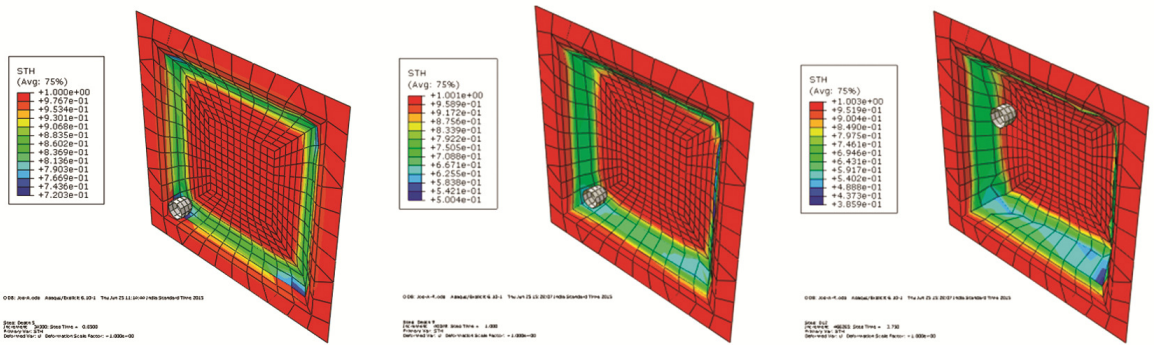

Fig. 7 — Numerical analysis of a square pyramid

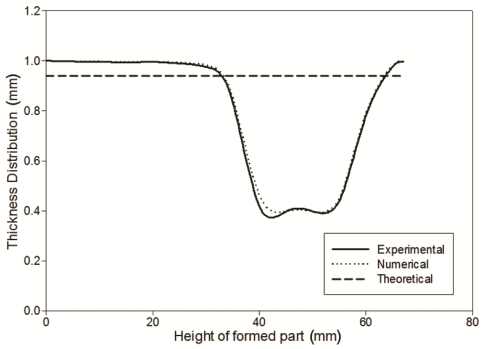

Fig. 8 — Comparison of thickness distribution on formed part

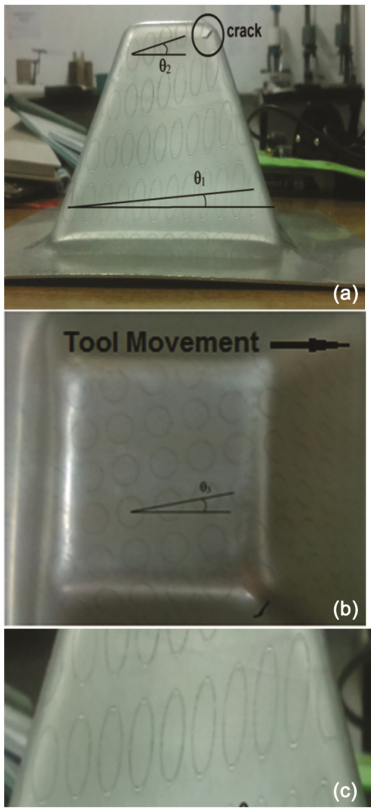

Fig. 9 — Twisting of etched circle grids (a) front view, (b) top view and (c) enlarged view of formed part

faces[23,24]. It can be noted that the maximum and minimum principal strains gradually raises from zero at the beginning upto the final stage and remains unchangeable. To validate the FEM model, the thickness distribution along the cross-section of the profile was obtained and compared with the obtained experimental one.

Comparison of thickness by means of experimental, theoretical and numerical analysis was shown in Fig. 8. Numerically obtained thickness distribution varies more with the theoretical value and closely agrees with the experimental values.

As a result, of tangential forces developed by the rotating tool over the work-piece, during the forming process, a twist of the material has been incorporated in the sheet metal. Twist of the sheet metal only becomes visible only when preformed markings were done prior to forming of the sheet[25,26]. The twist developed during forming process is shown in Fig. 9. At a higher drawing angle, close to the forming limit, a twist resulting opposite to the tool path movement can be observed. When the tool travels from the corner of the object, a redistribution of material takes place, resulting in excess deformation. When the tool moves forward, the corner acts a fulcrum. As the tool progresses, the material gets accumulated ahead of the tool tip resulting in decrease of deformation[27].

For a spindle speed (1931 rpm), tool feed (240 mm/min) and step depth (0.5 mm), the obtained twist angle was observed as 4° at the height of 10 mm as that of 14° at 65 mm. The angle at the top land was found a deviation of 9° from the axis of the circle grid and also a change in angle of 3° in the vertical direction on the formed part.

Conclusions

In this paper, formability performance of AA5052 alloy with 1 mm thickness and wall angle of 70° using incremental forming process is investigated. The sheet metal is formed at as it is condition. The following conclusions can be drawn from this study:

(i) The forming limit diagram and predicted thickness distribution obtained by single point incremental forming process was compared numerical simulations. Numerical results agreed reasonably well with the experimental results.

(ii) The targeted shape can be achieved at the corners and at the middle of the face there occurs a spring back effect. The spring back effect can be eliminated by optimizing the forming parameters toward the targeted shape.

(iii) It is evident from the experiment that the twist occurring increases is more as the forming depth increases due to accumulated material in front of the tool during forming. The twist can be eliminated by optimizing the tool path used for single point incremental forming.

References

1 Powell N & Andrew C, *J Eng Manuf Part B*, 205 (1992) 41-47.

2 Hagan E & Jeswiet J, *J Eng Manuf Part B*, 217 (2003) 213-225.

3 Hussain G, Gao L, Hayat N, Ziran X, *J Mater Process Technol*, 209 (2009) 4237-4242.

4 Kim Y H & Park J J, *J Mater Process Technol*, 130-131 (2002) 42-46.

5 Park J J & Kim J J, *J Mater Process Technol*, 40 (2003) 447-453.

6 Fratini L, Ambrogio G, Lorenzo R, Filice L & Micari F, *Ann CIRP*, 53(1) (2004) 207-210.

7 Filice L, Fratini L & Micari F, *Ann CIRP*, 51(1) (2002) 199-202.

8 Iseki H, *J Mater Process Technol*,-, 111 (2001) 150-154.

9 Jeswiet J R, Duflou J & Szekeres A, *Adv Mater Res*, 6-8 (2005) 449-456.

10 Mugendiran, V, Gnanavelbabu A & Ramadoss R, *Proc Eng*, 97 (2014) 1991-2000.

11 Ambrogio G, Costantino I, De Napoli L, Filice L, Fratini L & Muzzupappa M, *J Mater Process Technol*, 153-154 (2004) 501-507.

12 Duflou J.R, Tunçkol Y, Szekeres A & VanherckP, *J Mater Process Technol*, 189 (2007) 65-72.

13 Petek A, Kuzman K & Kopac J, *Arch Mater Sci Eng*, 35 (2009) 107-116.

14 Hussain G & Gao L, *Int J Mach Tools Manuf*, 47 (2007) 419–435.

15 Dejardin S, *J Mater Process Technol*, 210 (2010) 363-369.

16 Velmanirajan K, Anuradha K, Syed Abu Thaheer A, Ponalagusamy R & Narayanasamy R, *App Math Mod*, 38 (2014) 145-167.

17 Mugendiran V & Gnanavelbabu A, *Proc Eng*, 97 (2014) 1983-1990.

18 Loganathan C & Narayanasamy R, *Mater Sci Eng A*, 406 (2005) 229-253.

19 Ravindran R, Manonmani K & Narayanasamay R, *Mater Sci Eng A*, 507 (2009) 252-267.

20 Hu X, Lin Z Q, Li S H & Zhao Y X, *Mater Des*, 31 (2010) 1410-1416.

21 Martins P A F, Bay N, Skjoedt M & Silva M B, *Ann CIRP*, 57(1) (2008) 247-252.

22 Maria B Silva, Peter S Neilsen, Niels Bay & Martins P A F, *Int J Adv Manuf Tech*, 56 (2011) 893-903.

23 Junchao Li, Jianbiao Hu, Junjie Pan & Pei Gengg, *Int J Adv Manuf Tech*, 62 (2012) 981-988.

24 Shanmuganatan S P & Kumar V S S, *Mater Des,* 36 (2012) 546-569.

25 Vanhove H, Verbert J, Gu I, Vasilakos I & Duflou J R, *Int J Mater Form*, 3 (2010) 975-978.

26 Li Y, William J T D, Liu Z, Lu H & Paul A M, *J Mater Process Technol,* 221 (2015) 100-111.

27 Li Y, William J T D & Paul A M, *Int J Adv Manuf Technol*, 88 (2017) 255-267.